Metallophysics and Advanced Technologies
Металофіз. новітні технол.
Metallofiz. Noveishie Tekhnol.
2025, vol. 47, No. 4, pp. 391–404
https://doi.org/10.15407/mfint.47.04.0391
Reprints available directly from the publisher

PACS numbers: 61.43.Gt, 61.72.Ff, 81.05.Bx, 81.20.Ev, 81.20.Hy, 81.40.Jj, 81.70.Jb

On the Possibility to Manufacture Inconel-718 Alloy Products with Metal Injection Moulding Approach: Microstructure-Evolution Features and Main Characteristics

O. M. Ivasishin*, D. G. Savvakin*, O. D. Rud*, D. V. Oryshych*, I. M. Kirian*, A. M. Lakhnik*, V. I. Bondarchuk*, B. Kronowetter**, Yu. I. Torba***, V. G. Manzhos***

**G. V. Kurdyumov Institute for Metal Physics, N.A.S. of Ukraine, 36 Academician Vernadsky Blvd., UA-03142 Kyiv, Ukraine*
***KRONOWETTER Kunststoff- und Metalltechnik GmbH, Gewerbestrasse 32, Mitterfelden, D-83404 Germany*
****"Ivchenko-Progress" State Enterprise", 2 Ivanova Str., UA-69068 Zaporizhzhia, Ukraine*

The main features of manufacturing the Inconel-718 alloy products using mixture of Inconel-718 powder and an organic binder are studied. Using die-compacted and sintered feedstock, evolutions of microstructure and characteristics are studied during debinding, powder sintering and heat-treatment processing stages of metal injection moulding (MIM) manufacturing technique. The conditions and parameters ensuring formation of suitable microstructure and promising mechanical characteristics of final Inconel-718 material are determined. Nearly dense sintered material is formed on sintering, while post-sintering heat treatment ensures achievement of desirable phase composition. Hardness of 364 *HV*, tensile strength of about 900 MPa, and up

Corresponding author: Orest Mykhailovych Ivasishin
E-mail: ivas@imp.kiev.ua

Citation: O. M. Ivasishin, D. G. Savvakin, O. D. Rud, D. V. Oryshych, I. M. Kirian, A. M. Lakhnik, V. I. Bondarchuk, Yu. I. Torba, and V. G. Manzhos, On the Possibility to Manufacture Inconel-718 Alloy Products with Metal Injection Moulding Approach: Microstructure-Evolution Features and Main Characteristics, *Metallofiz. Noveishie Tekhnol.*, **47**, No. 4: 391–404 (2025). DOI: 10.15407/mfint.47.04.0391

to 17% elongation are achieved; such characteristics are promising to recommend MIM approach for manufacturing net-shape Inconel-718 alloy products.

Key words: metal injection moulding (MIM), Inconel-718, powder, binder, sintering, heat treatment, microstructure, mechanical properties.

Досліджено особливості одержання зразків стопу Inconel-718 із суміші порошку Inconel-718 та органічної зв'язки. З використанням пресування суміші у прес-формах і наступне спікання досліджено еволюції мікроструктури та характеристик під час технологічних операцій видалення зв'язки, спікання порошку та термічного оброблення, що відповідають операціям технології інжекційного формування та спікання виробів. Встановлено умови та параметри, що забезпечують формування бажаних мікроструктури та механічних характеристик кінцевого матеріялу. Під час спікання сформовано щільний матеріял, в той час як наступним термічним обробленням досягнуто його бажаного фазового складу, що забезпечує твердість у 364 *HV*, міцність під час випробувань на розтяг близько 900 МПа і видовження до 17%. Завдяки таким характеристикам метод інжекційного формування виробів може бути рекомендованим для виробництва деталів складної форми зі стопу Inconel-718.

Ключові слова: інжекційне формування, стоп Inconel-718, порошок, органічна зв'язка, спікання, термічне оброблення, мікроструктура, механічні характеристики.

(Received 2 April, 2025; in final version, 3 April, 2025)

1. INTRODUCTION

The development of materials and advanced technologies to manufacture improved aircraft engines is an important strategic task. As for today, the nickel-based alloys [1–2], including Inconel-718 one (52.50 Ni–18.50 Fe–9.00 Cr–5.10 Nb–3.00 Mo–0.50 Al–1.01 Ti–0.08 C, wt.%) are widely used for the manufacture of aircraft engine blades owing to high strength and corrosion resistance at temperatures up to 650–700°C.

The manufacturing approach should supply not only the required mechanical, service characteristics and high accuracy of a blade shape, but also provide sufficient cost-efficiency of the processing. Noted parts are usually produced by multistage technologies, including hot deformation of ingots and their mechanical processing (cutting), but this method results in significant losses of expensive material as waste. Moreover, Inconel-718 alloy ingots require specific heat treatment [3–5] to form the desired phase composition, microstructure, and, hence, the appropriate properties of final products, while low machinability and narrow temperature–speed range of plastic deformation for this material cause difficulties for mechanical processing

when obtaining net-shape products. The above noted problematic issues require the development of new cost-efficient methods of production of aviation parts with specified characteristics from Inconel-718 alloy.

The metal injection moulding (MIM) powder technology [6–8] is promising to overcome the problems mentioned above when obtaining net-shape products with determined structure and characteristics. MIM technologies include the forming of mixtures of metal powders and organic binders (feedstock) at relatively low pressures into workpieces of complex geometric shape, followed by the binder removal and sintering of the powders to obtain net-shape products. If necessary, the product is subjected to post-sintering heat and mechanical treatment. The expense of net-shape products manufactured using MIM technology is much lower than the cost of products manufactured using conventional technologies owing to a relatively simple set of technological operations for MIM processing and minimized material waste.

MIM technologies have made sufficient progress in the manufacture of stainless steels and ceramic products [6–8]. However, the production of Inconel-718 products by MIM requires preliminary adjustment of processing parameters, namely, proper selection of the binder removal regimes to avoid contamination of metal powders with binder remnants (C, O), development of sintering conditions to transform metal powders into massive (low-porous) sintered alloy and adjustment of heat treatment to form promising microstructure, phase composition, and, hence, desirable mechanical characteristics of final product.

As an alternative cost-efficient powder technology, ordinary die pressing and sintering of metal powders can be used for easy manufacturing of Inconel products [9] of relatively simple geometrical shape. However, powders produced with the gas-atomization method have a spherical shape and quenched microstructure, which commonly makes their die-compaction worse, and, thus, hinders to use of these powders for the press-and-sinter manufacturing technology. At the same time, mixing gas-atomized Inconel powder with organic binder used in MIM approach allows successful die-compaction of powder feedstock and further studies of all processing stages (debinding, sintering and heat treatment) which are similar to those in MIM processing. Therefore, such characteristic peculiarities of the MIM process as debinding, sintering and heat treatment, as well as the potential of the MIM approach for manufacturing Inconel-718 alloy products, can be studied using a simplified modelling approach based on die pressing and sintering of feedstock granules usually used in MIM.

This work is aimed to study the main features of pressing, debinding, sintering and heat treatment of the feedstock material consisting of Inconel-718 powder and an organic binder to evaluate the suitability of the MIM technique for manufacturing the Inconel-718 alloy products. To

fulfil one's production quota, it is necessary to determine the processing parameters that ensure the desired microstructure and mechanical properties of finished components.

2. MATERIALS AND EXPERIMENTAL PROCEDURE

Spherical powder of Inconel-718 alloy (Fig. 1*a*) produced with gas-atomization method was used as raw material in present study. The powder was mixed with PolyMIM binder [10] (Fig. 1*b*) to obtain feedstock granules 3–4 mm in size (Fig. 1*c*).

The feedstock granules were die-compacted at 620 MPa to obtain cylinders 10 mm in diameter, 12 mm in height. The debinding procedure included two stages, the first of which was washing in hot (70°C) water for 27 hours to evacuate water-solute components of the binder from the compacts. For the final debinding stage, the compacts were heated in a vacuum furnace to 800°C and exposed for 2 hours for evacuation of volatile components of PolyMIM binder. After that, the heating under vacuum was continued up to 1230°C and compacts were exposed for 2 hours at the noted temperature for powder sintering. As an alternative sintering option, the vacuumized heating chamber was filled with Argon above 970°C to perform sintering (1230°C, 2h) under inert atmosphere. During post-sintering cooling, the compacts were subjected to two-stage heat treatment at 720°C (2–4 h exposure) and 620°C (2–5 h exposure) to provide precipitation of strengthening phases.

The density of compacted and sintered samples was determined using precise mass and geometrical size measurements. The microstructure of initial powders and feedstock compacts at all stages of debinding and sintering was studied with a scanning electron microscope Tescan VEGA III equipped with a Brucker EDX analyser to evaluate local chemical composition and impurity content. The microstructure investigations were performed using polished surfaces of sintered and

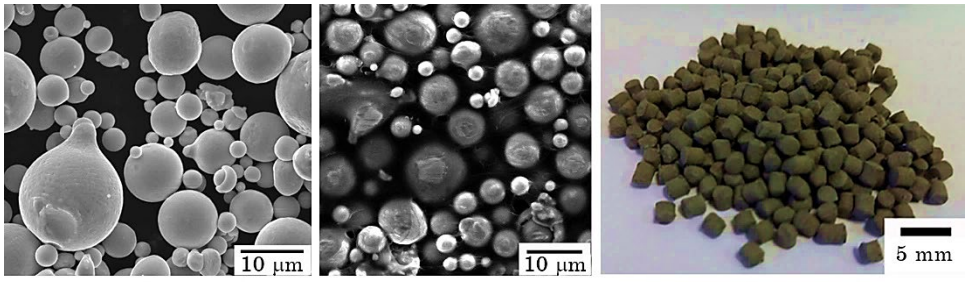

Fig. 1. Raw Inconel-718 powder (*a*), microstructure of powder-binder feedstock (*b*) and general view of feedstock granules (*c*).

heat-treated materials, as well as polished surfaces etched with a reagent based on a mixture of HCl, HNO_3 and acetic acids with glycerine to reveal microstructure constituents. Hardness tests (Wolpert 432 SVD tester) and tensile tests (Instron 3388 machine) were implemented to evaluate the mechanical characteristics of the material depending on sintering and heat treatment conditions.

The phase composition and crystal structures of the samples were examined by x-ray diffraction (XRD) technique using filtered MoK_α radiation. The diffraction spectra were collected using a PC-driven DRON-4 x-ray diffractometer (at 45 kV, 20 mA; in the 2θ-range of 5°–60° with a step of 0.05° and an acquisition time of 5 s per step) within the Bragg–Brentano geometry.

3. RESULTS AND DISCUSSION

Microstructure of the feedstock sample die-compacted at 620 MPa is presented in Fig. 2*a*. The spherical Inconel particles (Fig. 1*a*) were not deformed on die-compaction, but rearranged rather closer (Fig. 2*a*) than they were packed in the initial feedstock (see Fig. 1*b*) due to the applied compaction force. The surface of particles is covered and the voids between them are filled with binder. The measured density of die-compacted samples, which consisted of Inconel-718 powder and PolyMIM binder, was 5.80 g/cm^3, is lower than the standard density of bulk Inconel-718 alloy (8.19 g/cm^3 [11]) due to the high volume fraction of the light-weight binder and voids initially available in compacted samples. It should be noted, additional experiments on die-compaction of raw Inconel-718 powder without binder were not successful. As it was predicted, the smooth surface and high hardness of quenched Inconel-718 powder particles prevent die-compaction of the

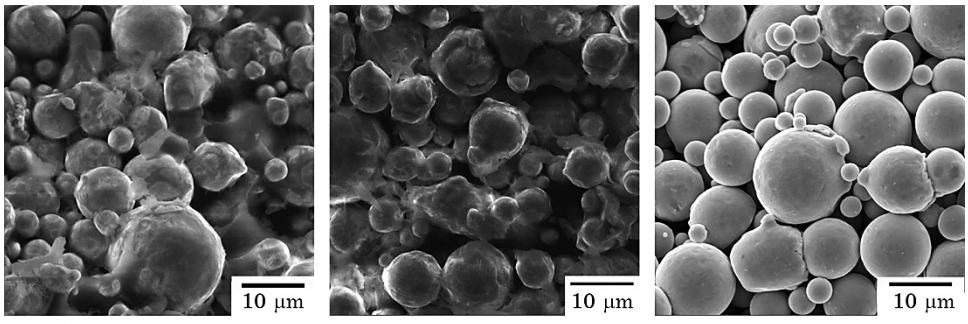

Fig. 2. Microstructures of die-compacted feedstock samples (*a*); after the first debinding stage (*b*); after the final debinding at 800°C within 2 hours and succeeding heating to 900°C in a vacuum furnace (*c*).

binder-free powder even at relatively high pressures (up to 950 MPa).

Washing compacted feedstock samples in hot water (first debinding stage) resulted in 3.2% mass loss due to partial removal of binder. Binder layers of reduced thickness were observed at powder surfaces with the appearance of hollow voids between powder particles (Fig. 2*b*). However, rearrangement of particles was not observed after the first debinding stage.

Microstructure of samples after the final stage of binder removal (800°C, 2h, vacuum) and further heating up to 900°C is shown in Fig. 2*c*. It is seen that, after debinding completion, the powder surface was clear, and no binder remnants were found in the voids between powder particles. However, sintering has not yet been developed; closer mutual rearrangement of particles and formation of sintering necks between particles have not been observed. Mass measurements revealed additional mass loss of 4.5% after the final debinding stage. So, feedstock compacts lost 7.7% of their initial mass during debinding.

Comparison of the chemical composition of powder particle surfaces for raw powder (before mixing with binder) and after debinding completion (Table 1, columns 1 and 2) has shown that no marked increase in carbon and oxygen impurities was observed after debinding. Hence, the binder has been successfully eliminated without dangerous contamination of powder particles. Despite that, the sintering process for powder particles was not developed, presumably, due to the presence of thin surface films with remnants of binder at the particle surfaces.

At this heating stage, the dangerous opportunity for fracture of pow-

TABLE 1. Chemical composition (mass.%) of Inconel powder particle surfaces in initial condition and after vacuum heating up to 900°C using different debinding regimes.

Element	Initial powder (before mixing with binder), %	Powder after debinding completion (heating up to 900°C using exposure at 800, 2h), %	Powder after continuous heating up to 900°C
Ni	52.7	52.4	52.2
Cr	19.0	19.3	19.5
Fe	18.9	18.5	18.2
Nb	4.1	4.1	5.1
Mo	1.4	2.7	1.3
Ti	1.0	1.0	1.1
Al	0.5	0.6	0.6
C	2.1	1.5	1.8
O	0.2	0.3	0.2

der compacts occurs. Thus, while the powder sintering has not yet been started, whole binder elimination creates dangerous reducing adhesion forces between powder particles in compacts and leads to the risk of compact fracture. For this reason, relatively quick heating of compacts up to 900°C was tested to preserve the binder remnants and related bonding forces between adjacent powder particles up to temperatures sufficiently high for sintering activation. To test the binder effect on the shape retention of the pressed compacts within sintering, we performed continuous heating at 5 K/min up to 900°C (without exposure at 800°C for debinding). Really, for this case, measured mass loss was approximately 7.2%, *i.e.*, 0.5% lower than for the debinding scheme including 2 hours exposure at 800°C, thus, suggesting preservation of binder remnants on the surfaces of Inconel particles. However, powder compacts cooled from 900°C after such modification of heating and debinding scheme (Table 1, column 3) did not demonstrate noticeable change of chemical composition of particles surface, while any features for improved bonding of powder particles were not observed (Fig. 3). So, debinding scheme using continuous heating was discarded due to absence of positive influence on compact strength.

Temperature of 1230°C sufficiently activates the sintering of powder particles. Exposure for 2 hours at 1230°C resulted in 22% shrinkage of powder samples and formation of quite dense Inconel-718 material. Measured density reached 7.8 g/cm^3 that corresponds to 95% of theoretical value. However, important factor is sintering environment, which affects chemical composition of sample surface. Vacuum sintering re-

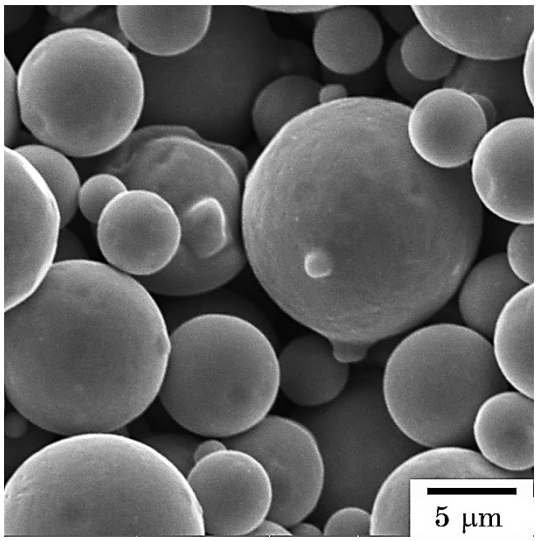

Fig. 3. Surface of powder particles after fast heating up to 900°C.

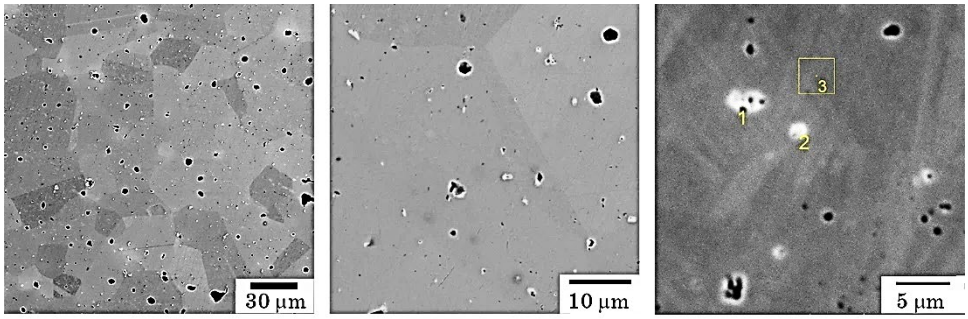

Fig. 4. As-sintered microstructure of Inconel-718 alloy (*a*–*b*) and microstructure features (*c*) used for local EDX analysis (Table 2).

sulted in more than 4% losses of chromium at surface and sub-surface areas of the samples due to evaporation of this alloying element at high temperatures. Evaporation of chromium in vacuum at high temperatures changes the chemical composition, which, in turn, affects critical characteristics of the alloy surface. To avoid risk of characteristics' degradation, argon atmosphere looks like more promising than vacuum. Hence, argon atmosphere has been selected as sintering environment to protect Inconel-718 surface. However, initial stages of heating were implemented in vacuum to complete debinding process, after that heating chamber was filled with Ar at temperature of 1000°C.

The as-sintered sample microstructure (Fig. 4*a*, *b*) consisted of uniform grains 30–50 μm in size with residual pores (up to 5–10 μm) and fine (1–2 μm) precipitations located near grain boundaries and inside grains. Local chemical analysis (Fig. 4*c*, Table 2) revealed that the chemical composition of alloy matrix (area 3, Table 2) is rather similar to total alloy composition, while precipitations are considerably enriched with Nb, Ti, Mo and C. The precipitations were identified as (Nb, Ti, Mo)C carbides, similarly to NbC and (Nb, Ti)C carbides [3, 12–14] earlier observed for Inconel-718 alloy. However, taking into consideration approximately equal energy values for NbK_β and MoK_α x-ray irradiation, measured enhanced Mo content (6–7%) in precipitations looks doubtful in our case.

X-ray diffraction study confirmed two-phase composition of sintered alloy (Fig. 5*a*): main peaks of γ (f.c.c.) nickel–iron–chromium-based matrix were observed together with weak peaks of (Nb, Ti)C carbide phase. Following reference data [3, 12, 13], undesirable Laves phase $(Ni, Cr, Fe)_2(Nb, Mo, Ti)$ and δ (Ni_3Nb) phase, which negatively affect mechanical characteristics, can be formed at temperatures below 1100°C in Inconel-718 too. However, these phases were not observed for as-sintered condition because they did not exist at sintering

TABLE 2. Total and local chemical composition of alloy matrix and precipitation phase after sintering and subsequent not-controlled furnace cooling condition.

Element, wt.%	Total composition	Local compositions (see Fig. 4*c*)		
		1 (precipitation phase)	2 (precipitation phase)	3 (alloy matrix)
Ni	52.2	12.3	19.6	51.9
Cr	18.9	5.5	8.3	19.1
Fe	17.8	4.6	7.1	18.1
Nb	4.0	53.1	43.1	3.7
Mo	2.9	7.4	6.2	2.9
Ti	1.0	6.8	7.5	1.0
Al	0.6	0.5	0.3	0.5
C	2.3	8.0	7.2	2.5
O	0.3	0.9	0.6	0.2

temperature of 1230°C and were not formed on relatively fast post-sintering cooling in furnace.

Hardness of sintered alloy was relatively low at the level of 192 *HV*, which can be explained with not optimized phase composition of alloy formed during sintering and subsequent not controlled furnace cooling condition.

To achieve required set of hardness and tensile characteristics, heat

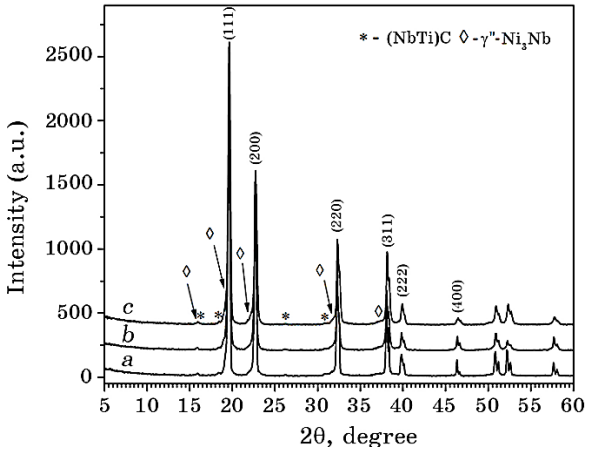

Fig. 5. X-ray diffraction patterns of sintered (*a*) and aged Inconel samples at 720°C + 620°C during 2+2 hours (*b*) and 4+5 hours (*c*).

treatment after sintering was used. The procedures of compact debinding in vacuum, and subsequent sintering and heat treatment under Argon atmosphere were successively performed within the one heating cycle, thus, promoting cost-efficiency of processing.

Strengthening heat-treatment regimes for Inconel-718 alloy [3, 11, 15] recommend annealing at temperatures of about 980–1200°C, subsequent fast cooling, and relatively long-time ageing consisted of two consecutive stages: 720°C, 8 h and 620°C, 8–10 h. Such heating scheme allow to avoid formation of undesirable phases like Laves phase and δ-Ni_3Nb phase, while two-stage ageing at noted temperatures ensures formation of highly dispersed strengthening γ′-Ni_3(Ti,Al) and γ″-Ni_3Nb precipitations in γ-matrix. In our case, direct ageing during post-sintering cooling was used to precipitate disperse γ′-Ni_3(Ti,Al) and γ″-Ni_3Nb phases in alloy matrix and, hence, to improve hardness and ten-

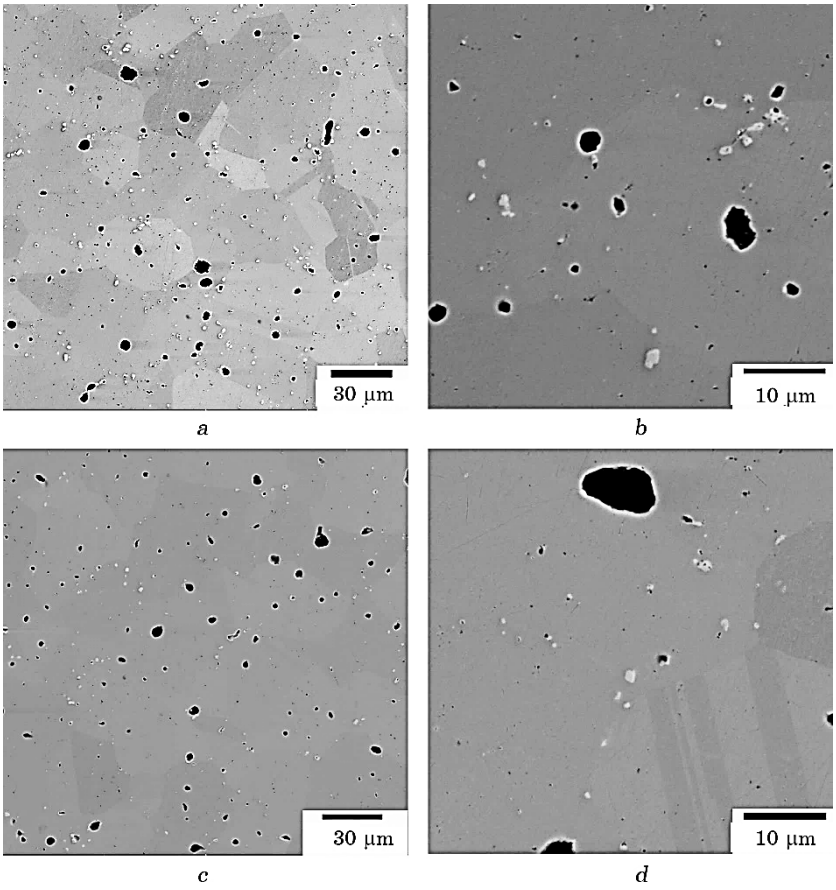

Fig. 6. SEM microstructures after ageing 720°C + 620°C during 2+2 hours (*a*, *b*) and 4+5 hours (*c*, *d*).

sile characteristics. Usually, the most important microstructure changes take place during first stages of the ageing. For this reason, two ageing regimes of different durations: 2+2 hours and 4+5 hours at recommended temperatures 720°C and 620°C were tested to evaluate microstructure evolution and kinetic of mechanical characteristics change.

Aged microstructures are shown in Fig. 6. SEM observations did not detect obvious changes in microstructure compared to as-sintered condition (Fig. 4); transformation or dissolution of initially presented carbide particles were not observed the same as precipitation of new phases. Maps of alloying elements redistribution (Fig. 7) show that particles presented in aged Ni–Fe–Cr-based matrix are enriched with Nb, Ti, Mo and C, being quite similar to (Nb,Ti)C carbides observed for as-sintered condition, which did not undergo marked changes during subsequent ageing. Furthermore, surface of some pores observed in microstructure are enriched with Nb, Ti, Mo and C (Fig. 7), hence, these pores can be identified as remnants of brittle carbide particles, which were fractured and fell out during polishing operations. However, despite absence of obvious microstructure changes (Figs. 4, 6), x-ray diffraction analysis (Fig. 5) demonstrated some differences in phase composition for as-sintered and sintered+aged materials. Sintered+aged conditions (Fig. 5*b*, *c*), in addition to smartly prominent x-ray diffraction peaks corresponding to γ (f.c.c.) nickel–chromium–

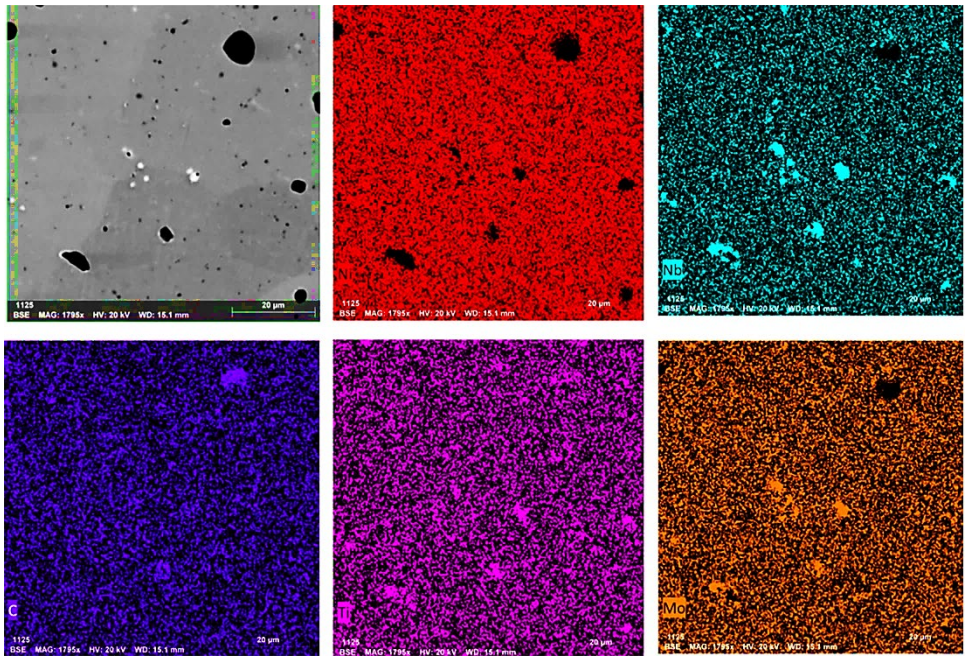

Fig. 7. Alloying element map distribution for sample aged 720°C 4 h + 620°C, 5 h.

iron-based matrix and f.c.c.-(Nb,Ti)C carbide phase, demonstrate weak peaks belonging to γ''-Ni_3Nb phase. The γ''-Ni_3Nb phase has an ordered body-centred tetragonal (b.c.t.) $D0_{22}$-crystalline structure, which belongs to the $I4/mmm$ space group (No. 139) [16]. Also, the difference in x-ray diffraction patterns for as-sintered and aged conditions is slightly increased wide of diffraction peaks of γ (f.c.c.) matrix and displacement of peaks positions towards higher angles with increased ageing duration. Such result can be interpreted as gradual decrease in interplanar distance and appearance of some stresses in γ (f.c.c.) matrix with long-time ageing due to precipitation of phases with another chemical composition, γ''-Ni_3Nb phase in our case like it was observed in [13] due to δ-Ni_3Nb phase precipitation.

The ageing resulted in continuous hardness growth with increase in ageing duration. The hardness was noticeably increased after 720°C, 2 h plus 620°C, 2 h ageing, achieving 333 *HV*. Increase in ageing duration to 4+5 hours at corresponding temperatures resulted in further hardness growth up to 364 *HV*.

The reference data proofs that reinforcing γ''-Ni_3Nb and γ'-$Ni_3(Ti,Al)$ phases in alloy matrix precipitate as nanosize particles (10–200 nm) [3, 12–14], observation of which needs high-resolution SEM equipment. So, noted phases can be observed, when particle growth and development of coagulation result in formation of particles of sufficiently high sizes. Presumably, during used ageing regimes the nuclei of reinforcing particles were formed in γ (f.c.c.) Ni–Cr–Fe-based matrix, their weak traces can be detected with x-ray diffraction analysis (Fig. 5*b*, *c*), but formation of highly-disperse nuclei hardly can be observed with used SEM technique. On another hand, formation of high-disperse γ''-Ni_3Nb and γ'-$Ni_3(Ti,Al)$ nuclei in γ (f.c.c.) matrix is confirmed with observed increase in hardness from 192 *HV* to 364 *HV*. The kinetic of precipitation process is slow and formation of coarse precipitations visible with SEM technique will take relative long time ageing, which duration is higher than used in present study.

Preliminary tensile test of aged material (Fig. 8) revealed sufficient strength/ductile characteristics promising for further development and adaptation of MIM approach in industry to produce Inconel-718 products. At the same time, additional experiments are necessary to adjust processing parameters for further optimization of sintered/aged material microstructure and properties.

4. CONCLUSIONS

1. Feedstock granules consisted of Inconel-718 powder and PolyMIM binder were successfully used in press-and-sinter approach for manufacturing bulk Inconel-718 products. The main processing parameters ensuring formation of suitable microstructure and mechanical characteristics

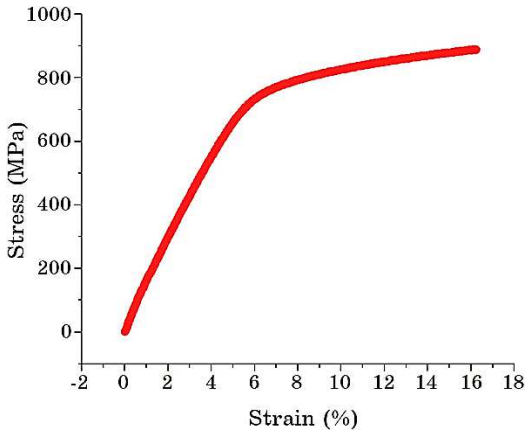

Fig. 8. Stress–strain tensile curve of sintered and heat treated Inconel-718 material.

of final material were determined and recommended to be used in MIM processing to achieve desired characteristics of net-shape Inconel-718 products manufactured by MIM.

2. Two-stage debinding of powder compacts (washing in hot water and subsequent vacuum exposure at 800°C) ensured formation of clean powder surfaces not contaminated with binder remnants, however, sintering of powder particles developed at temperatures quite above 900°C.

3. Sintering at 1230°C under argon atmosphere is recommended because of vacuum sintering resulted in Cr evaporation from surface of the powder compacts. Sintering ensures formation of nearly-dense microstructure of Inconel-718 alloy, while post-sintering heat treatment increases the material hardness owing to precipitation of nanoscale strengthening γ'-$Ni_3(Ti,Al)$ and γ''-Ni_3Nb phases in γ (f.c.c.) matrix.

4. Hardness of 364 *HV*, tensile strength of about 900 MPa, and up to 17% elongation were achieved with post-sintering heat treatment; such characteristics are promising to recommend MIM approach for manufacturing Inconel-718 alloy products.

ACKNOWLEDGEMENT

This work was supported by a grant №2023.04/0058 of the National Research Foundation of Ukraine.

REFERENCES

1. A. Enes and A. Gürsel, *Period. Eng. Nat. Sci.*, **3**, No. 1: 15 (2015).
2. R. J. Smith, G. J. Lewi, and D. H. Yates, *Aircraft Engineering and Aerospace*

Technology, **73**, No. 2: 138 (2001).
3. W. M. Tucho, P. Cuvillier, A. Sjolyst-Kverneland, and V. Hansen, *Mater. Sci. Eng. A*, **689**: 220 (2017).
4. R. Cozar and A. Pineau, *Metall. Trans.*, **4**: 47 (1973).
5. M. Sundararaman, P. Mukhopadhyay, and S. Banerjee, *Metall. Trans. A*, **23**: 2015 (1992).
6. R.M. German, *Handbook of Metal Injection Molding, 1 – Metal Powder Injection Molding (MIM): Key Trends and Markets* (Ed. Donald F. Heaney) (Woodhead Publishing: 2012).
7. F. T. Teferi and A. A. Tsegaw, *Advances of Science and Technology. ICAST 2021. Lecture Notes of the Institute for Computer Sciences, Social Informatics and Telecommunications Engineering. Vol. **412*** (Cham: Springer: 2022).
8. I. P. Widiantara, R. A. Kurnia Putri, D. I. Han, W. Bahanan, E. H. Lee, Ch. H. Woo, J.-H. Kang, J. Ryu, and Y. G. Ko, *Materials*, **16**, No. 6: 2516 (2023).
9. G. H. Gessinger and M. J. Bomford, *Int. Met. Rev.*, **19**, No. 1: 51 (1974).
10. www.polymim.com
11. https://www.upmet.com/sites/default/files/datasheets/718.pdf
12. A. Chamanfar, L. Sarrat, M. Jahazi, M. Asadi, A. Weck, and A. K. Koul, *Materials and Design*, **52**: 791 (2013).
13. M. Dehmas, J. Lacaze, N. Niang, and B. Viguier, *Adv. Mater. Sci. Eng.*, **2011**, No. 3: 1 (2011).
14. C.-M. Kuo, Y.-T. Yang, H.-Y. Bor, C.-N. Wei, and C.-C. Tai, *Mater. Sci. Eng. A*, **510–511**: 289 (2009).
15. S. Ghosh, S. Yadav, G. Das, *Mater. Lett.*, **62**: 2619 (2008).
16. D. K. Gorai and T. K. Kundu, *IOP Conf. Series: Mater. Sci. Eng.*, **338**: 012041 (2018).